The practical MFCAV Riemann solver is applied to a new cell-centered Lagrangian method

Yan Liu, Weidong Shen, Dekang Mao, Baolin Tian

Abstract—The MFCAV Riemann solver is practically used in many Lagrangian or ALE methods due to its merit of sharp shock profiles and rarefaction corners, though very often with numerical oscillations. By viewing it as a modification of the WWAM Riemann solver, we apply the MFCAV Riemann solver to the Lagrangian method recently developed by Maire. P. H et. al.. The numerical experiments show that the application is successful in that the shock profiles and rarefaction corners are sharpened compared with results obtained using other Riemann solvers. Though there are still numerical oscillations, they are within the range of the MFCAV applied in onther Lagrangian methods.

Keywords—cell-centered Lagrangian method, approximated Riemann solver, HLLC Riemann solver

I. INTRODUCTION

LAGRANGIAN hydrodynamics algorithm have been widely used for a long time in the solution of complex problem of fluid flow. Lagrangian schemes are characterized by a mesh that follows the fluid flow. By this mean, these methods deal with interfaces in a natural manner. The main numerical difficulty lies in the node motion discretization, especially for multidimensional cases. There are two well-known finite volume schemes in Lagrangian formulism. One is the discretization on staggered grid proposed by von Neumann and Richtmyer, where the momentum is defined at the nodes and the other thermodynamic variables(density, pressure and specific internal energy) are all cell-centered, so that the vertex velocity can be computed by a most natural way[2][3]. It is based on an internal energy formulations. In its initial version, this scheme was not conservative and it admitted numerical spurious modes. Moreover, since a decade, many improvements have been done in order to solve the previous problems, for example, Caramana and Shashkov[4]show that with an appropriate discretization of the subzonal forces resulting from subzonal pressures, hourglass motion and spurious vorticity can be eliminated.

An alternative to the staggered discretization is to use a conservative cell-centered discretization, in this method all the variables are defined in the cell centered [5], [6]. In this

Yan Liu is with Laboratory of computational Physics, Institute of Applied physics and computational mathematics, Beijing,100094,China (phone:010-59872169; e-mail: yan_liu@ iapcm.ac.cn).

Dekang, Mao is with Shanghai University, Shanghai, China (e-mail: dkmao@ staff.shu.edu.cn).

classical cell-centered scheme, flux across the boundary of the cell is computed by solving exactly or approximated a one-dimensional Riemann problem in the direction normal to the boundary. The main problem with this type of method lies in the fact that the node velocity needed to move the mesh cannot be directly calculated. In [8] and [9], the node velocity is computed via a special least squares procedure. It consists in minimizing the error between the normal velocity coming from the Riemann solver and the normal projection of the vertex velocity. It turns out that it leads to an artificial grid motion, which requires a very expensive treatment. Moreover, with this approach the flux calculation is not consistent with the node motion.

Recently, a new two-dimensional Lagrangian cell-centered scheme, which is conservative and entropy consistent, of the finite volume type is derived in [1]. The vertex velocity and the numerical fluxes through the cell interfaces are not computed independently as usual but in a consistent manner with an original solver located at the nodes. The main new feature of the algorithm is the introduction of four pressures on each edge, two for each node on each side of the edge. This extra degree of freedom allows them to construct such a nodal solver that face fluxes and the nodal velocities are all evaluated in a coherent manner. The nodal solver is constructed by satisfying the global balance of momentum and entropy inequality. From the nodal solver the vertex velocity can be determined by the weighted least square method. In[1], the weight is set to the acoustic impedance then the velocity along the normal direction of the cell interfaces is just the velocity of the weak wave approximated Riemann solver(WWAM). But different approximated Riemann solver behaves different numerical features which can obtain different efficiency of the numerical scheme for the fluid flows. Because WWAM can only simulate the problems in which the shocks are not complex. So we hope to analyze some practical approximated Riemann solvers for the new Lagrangian method and to simulate complex problems. We use several approximated Riemann solvers, for example HLLC Riemann solver, Duckowicz double shock Riemann solver and MFCAV Riemann solver, under the condition that the weights of the Riemann invariants along the normal direction of the cell faces are still set to the acoustic impedance, to simulate the Sod shock tube problem, but the results do not approximate to the accurate solution. So we know that the Riemann solvers discussed above are not applied to the new Lagrangian method directly. Based on the consideration above, we study deeply how to develop and

World Academy of Science, Engineering and Technology
International Journal of Mathematical and Computational Sciences
Vol:5, No:5, 2011

apply the Riemann solvers discussed above to the new Lagrangian method. For Duckowicz double shock Riemann solver which is second order accuracy and very complex, we don't consider it in this paper. But now we have found the techniques to apply HLLC and MFCAV Riemann solver to the new Lagrangian method successfully and obtain good results. But the technique for HLLC Riemann solver is simpler compared to the MFCAV Riemann solver, we don't consider it in this paper, we refer the readers to see [15] for details. In this paper we will discuss deeply how to apply MFCAV Riemann solver to the new Lagrangian method.

The rest of this paper is organized as follows: In section2, we simply recall the new Lagrangian method. Then we analyze how to construct the nodal solver for general approximated Riemann solvers to be adapted to the new Lagrangian method. In section4, we validate our new scheme with some test cases, and the numerical results demonstrate the robustness and the accuracy of the method. Finally the conclusion is given in section 5.

II. SIMPLY RECALL THE NEW LAGRANGIAN METHOD

A. Governing Equation

The gas dynamics equations for an inviscid compressible fluid equations written in Lagrangian formalism in integral form is

$$
\begin{cases}
\dfrac{d}{dt}\int_{\Omega(t)} \rho\, d\Omega = 0, \\[2mm]
\dfrac{d}{dt}\int_{\Omega(t)} d\Omega - \int_{\partial\Omega(t)} V\cdot N d\partial\Omega = 0, \\[2mm]
\dfrac{d}{dt}\int_{\Omega(t)} \rho V d\Omega + \int_{\partial\Omega(t)} PN d\partial\Omega = 0, \\[2mm]
\dfrac{d}{dt}\int_{\Omega(t)} \rho E d\Omega + \int_{\partial\Omega(t)} PV\cdot N d\partial\Omega = 0,
\end{cases}
\tag{1}
$$

where ρ, E and $V=(u,v)$ denote the density, the specific total energy and the fluid velocity respectively. We denote by $e = E - 0.5V\cdot V$ the specific internal energy and P the pressure given by the equation of state $P = P(\rho,e)$. Ω is a control-volume and $\partial\Omega$ is the boundary of Ω, N is the unit outward normal to $\partial\Omega$ and dl is the length element on $\partial\Omega$, see [1]and [13] for the details. Let m_Ω denotes the mass of fluid enclosed in Ω. Let us introduce the area of domain Ω:

$$
A_\Omega = \int_\Omega d\Omega \cdot
$$

We define the density $\rho_\Omega = m_\Omega / A_\Omega$ and the specific volume $\tau_\Omega = 1/\rho_\Omega$, we also define the mass averaged velocity and total energy

$$
V_\Omega = \frac{1}{m_\omega}\int_\Omega \rho V d\Omega
$$
,

$$
E_\Omega = \frac{1}{m_\omega}\int_\Omega \rho E d\Omega
$$

Then (1)can be written in such form

$$
\begin{aligned}
m_\omega \frac{d}{dt} T_\Omega - \int_{\partial\Omega} V\cdot N dl = 0 \\[2mm]
m_\omega \frac{d}{dt} V_\Omega - \int_{\partial\Omega} PN dl = 0 \\[2mm]
m_\omega \frac{d}{dt} E_\Omega - \int_{\partial\Omega} PV\cdot N dl = 0
\end{aligned}
\tag{2}
$$

B. Spatial Approximation

Apply the classical finite volume scheme to discrete(2),see Fig.1,Ω_i is a polygonal cell whose vertices are denoted by $M_r, r = 1,...,R(i)$. We denote by R(i) the number of vertices(or faces) of the cell Ω_i. The vertices are indexed counter clockwise. $L_{r,r+1}, T_{r,r+1}$ and $N_{r,r+1}$ represents the length, the unit tangent vector and the unit outward normal vector of any edge $[M_r, M_{r+1}]$ respectively. The fluid in cell Ω_i is described by the discrete variables (τ_i, V_i, E_i), respectively the averaged specific volume, velocity and specific total energy. Then (2) can be discrete as (3), see [1] for details.
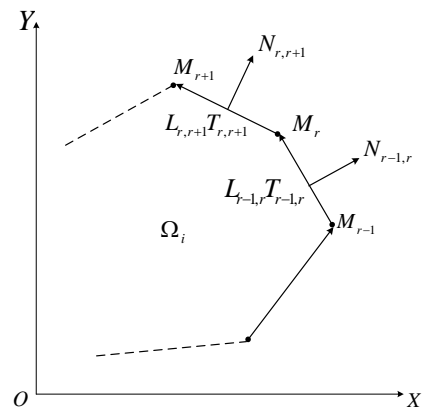

Fig.1: Notations

$$
m_i \frac{d}{dt}\tau_i - \sum_{r=1}^{R(i)} L_{r,r+1} V^*_{r,r+1} \cdot N_{r,r+1} = 0
\tag{3-(i)}
$$

$$
m_i \frac{d}{dt} V_i + \sum_{r=1}^{R(i)} L_{r,r+1} P^*_{r,r+1} N_{r,r+1} = 0
\tag{3-(ii)}
$$

$$
m_i \frac{d}{dt} E_i + \sum_{r=1}^{R(i)} L_{r,r+1} (PV)^*_{r,r+1} \cdot N_{r,r+1} = 0
\tag{3-(iii)}
$$

For the classical Godunov method [5], [6], the normal velocity $V^*_{r,r+1} \cdot N_{r,r+1}$ is determined by a one-dimensional Riemann solver at faces. An immediate consequence is of course the conservation of the finite volume method (3).

World Academy of Science, Engineering and Technology
International Journal of Mathematical and Computational Sciences
Vol:5, No:5, 2011

Nevertheless, one drawback of such a method is that the Riemann solver provides only edge–centered normal component velocities, whereas the velocities of vertexes are needed to move the mesh. It is impossible, in the general case, to construct a node velocity whose projection in the normal direction of each face around the node is equal to the Riemann normal component velocity. For this reason most of the known methods consist of solving an optimization problem such as that in the CAVEAT code [8] and [9]. Thus, the variation of cell areas must be recomputed to keep the coherent with vertex motion.

In [1] a new method is proposed , where the vertex velocities   are at first evaluated using some still-to-define solver. The face velocity are then computed from node velocity by

$$V_{r,r+1}^* = \frac{1}{2}(V_r^* + V_{r+1}^*), \qquad (4)$$

where (4) can be obtained by geometry conservation law and (3)-(i), so the flux of cell faces and the flux at node are in a coherent manner.

Similarly, the pressure and energy of the cell faces are discrete as

$$P_{r,r+1}^{*,i} = \frac{1}{2}(P_{r,r+\frac{1}{2}}^{*,i} + P_{r+\frac{1}{2},r+1}^{*,i})$$

$$(PV)_{r,r+1}^{*,i} = \frac{1}{2}(P_{r,r+\frac{1}{2}}^{*,i} V_r^* + P_{r+\frac{1}{2},r+1}^{*,i} V_{r+1}^*)$$

where the pressure $P_{r,r+1/2}^{*,i}$ and $P_{r+1/2,r+1}^{*,i}$ represents the pressure on the half face $[M_r, M_{r+1/2}]$ and $[M_{r+1/2}, M_{r+1}]$ see from the cell Ω_i, see Fig.2. Then equation (3) can be shifted to such form

$$m_i \frac{d}{dt}\tau_i - \sum_{r=1}^{R(i)} \frac{1}{2} L_{r,r+1}(V_r^* + V_{r+1}^*) \cdot N_{r,r+1} = 0$$

$$m_i \frac{d}{dt}V_i + \sum_{r=1}^{R(i)} \frac{1}{2}(L_{r-1,r} P_{r-\frac{1}{2},r}^{*,i} N_{r-1,r} + L_{r,r+1} P_{r,r+\frac{1}{2}}^{*,i} N_{r,r+1}) = 0 \qquad .(5)$$

$$m_i \frac{d}{dt}E_i + \sum_{r=1}^{R(i)} \frac{1}{2}(L_{r-1,r} P_{r-\frac{1}{2},r}^{*,i} N_{r-1,r} + L_{r,r+1} P_{r,r+\frac{1}{2}}^{*,i} N_{r,r+1}) \cdot V_r^* = 0$$
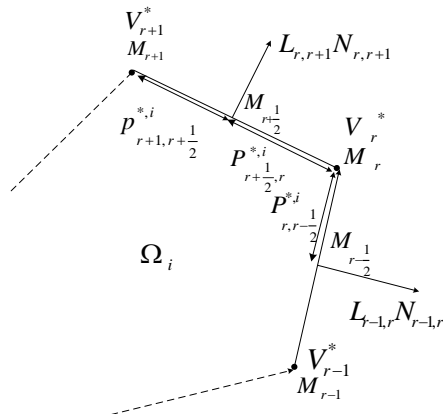

Fig.2 Pressures at faces

C. Construction of a Solver at the Vertices

In (5), the conservation equation is shifted to the form of vertex flux from the form of face flux. The key point is how to compute the vertex pressure $(P_{r,r+1/2}^{*,i}, P_{r+1/2,r+1}^{*,i})$ and vertex velocity V_r^*. In [1], the vertex pressure $(P_{r,r+1/2}^{*,i}, P_{r+1/2,r+1}^{*,i})$ and vertex velocity V_r^* are computed by constructing solver at the vertices under the conditions of global balance of momentum and satisfying entropy inequality. We simplify describe it, see [1] for details.

Notations around vertex M_q is defined as in Fig.3. The global balance of momentum is shifted to vertex, then it takes as such form

$$\frac{d}{dt}(\sum_{i=1}^{I} m_i V_i) = \sum_{q=1}^{Q} \sum_{k=1}^{K(q)} \frac{1}{2}(L_k P_{q,k}^{*,k} N_k^k + L_{k+1} P_{q,k+1}^{*,k} N_{k+1}^k) = 0 \cdot \qquad (6)$$

The (global) conservation of momentum is satisfied provided the right hand side vanishes. A sufficient condition is

$$\sum_{k=1}^{K(q)} \frac{1}{2}(L_k P_{q,k}^{*,k} N_k^k + L_{k+1} P_{q,k+1}^{*,k} N_{k+1}^k) = 0 \, , \qquad (7)$$

This summation is done over all the cells k surrounding vertex M_q. Relation (7) can be interpreted as the local equilibrium of vertex M_q under pressure force. This is also a local conservation relation. The condition (7) also implies the global conservation of total energy.

From the entropy condition, such relation is obtained

$$m_i T_i \frac{d}{dt}\sigma_i = m_i(\frac{d}{dt}\varepsilon_i + P_i \frac{d}{dt}\tau_i) = \qquad (8)$$

$$\sum_{r=1}^{R(i)} \frac{1}{2}\left[L_{r-1,r}(P_i - P_{r-\frac{1}{2},r}^{*,i})N_{r-1,r} + L_{r,r+1}(P_i - P_{r,r+\frac{1}{2}}^{*,i})N_{r,r+1} \right] \cdot (V_r^* - V_i)$$

where σ_i and ε_i are the entropy, the internal energy in cell Ω_i respectively. T_i is the cell average temperature.

A sufficient condition for the right hand side of this relation to be positive is

$$P_i - P_{r-\frac{1}{2},r}^{*,i} = \alpha_i (V_r^* - V_i) \cdot N_{r-1,r}, r = 1...R(i)$$

$$P_i - P_{r,r+\frac{1}{2}}^{*,i} = \alpha_i (V_r^* - V_i) \cdot N_{r,r+1}, r = 1...R(i)$$

$\qquad (9)$

where α_i is a positive coefficient that has the dimension of a mass flux. These tworelation can be interpreted as Riemann invariants along the directions $N_{r-1,r}$ and $N_{r,r+1}$. If we rewrite the condition (9) using notations around a generic vertex M_q, we obtain

$$\begin{cases} P_{q,k}^{*,k} = P_k + \alpha_k (V_q^* - V_k) \cdot N_k^{k-1} \\ P_{q,k}^{*,k-1} = P_{k-1} - \alpha_{k-1} (V_q^* - V_{k-1}) \cdot N_k^{k-1} \end{cases} . \qquad (10)$$

If we shift index ($k \to k-1$) in the second term of (6) and

World Academy of Science, Engineering and Technology
International Journal of Mathematical and Computational Sciences
Vol:5, No:5, 2011

get

$$\sum_{k=1}^{K(q)} L_k (P_{q,k}^{*,k} - P_{q,k}^{*,k-1}) N_k^{k-1} = 0 , \qquad (11)$$

where we have used $N_k^k = -N_k^{k-1}$.

After substitution of (10) in (11), we obtain the following equation

$$\sum_{k=1}^{K(q)} L_k (\alpha_{k-1} + \alpha_k) \left[V_q^* \cdot N_k^{k-1} - \frac{P_{k-1} - P_k + \alpha_{k-1} V_{k-1} \cdot N_k^{k-1} + \alpha_k V_k \cdot N_k^{k-1}}{\alpha_{k-1} + \alpha_k} \right] N_k^{k-1} = 0 \qquad (12)$$

If we set

$$V_k^* = \frac{P_{k-1} - P_k + \alpha_{k-1} V_{k-1} \cdot N_k^{k-1} + \alpha_k V_k \cdot N_k^{k-1}}{\alpha_{k-1} + \alpha_k} , \qquad (13)$$

V_k^* is the normal velocity given by the classical one dimensional acoustic Riemann solver for face $[M_q, M_k]$

$$\sum_{k=1}^{K(q)} L_k (\alpha_{k-1} + \alpha_k) \left[V_q^* \cdot N_k^{k-1} - V_k^* \right] N_k^{k-1} = 0 . \qquad (14)$$

A straightforward calculation shows that the left hand side of this last equation is the gradient of the following quadratic functional

$$F(u_q^*, v_q^*) = \sum_{k=1}^{K(q)} L_k (\alpha_{k-1} + \alpha_k) \left[V_q^* \cdot N_k^{k-1} - V_k^* \right]^2 , \qquad (15)$$

where (u_q^*, v_q^*) denotes the components of V_q^* . Consequently, the solution of equation (12) reaches the minimum of the fuctional $F(u_q^*, v_q^*)$. Hence, it appears that the nodal velocity V_q^* is obtained from a weighted least squares procedure.
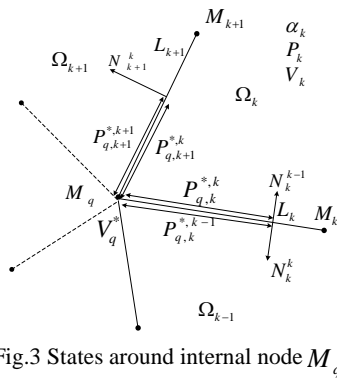

Fig.3 States around internal node M_q

III. THE DEVELOPMENT AND APPLICATION OF THE MFCAV RIEMANN SOLVER

From the above discussion , we see that for (10) and (12), the key point is how to select the weight α_k . In [1] α_k is set to the acoustic impedance, then (13) is just the velocity of the weak wave approximated Riemann solver(WWAM)

$$\vec{V} \cdot n_{j-\frac{1}{2},k} = \frac{(\rho c \vec{V} \cdot n)_{j-\frac{1}{2},k+\frac{1}{2}} + (\rho c \vec{V} \cdot n)_{j-\frac{1}{2},k-\frac{1}{2}}}{(\rho c)_{j-\frac{1}{2},k+\frac{1}{2}} + (\rho c)_{j-\frac{1}{2},k-\frac{1}{2}}} - \frac{\Delta t (P_{j-\frac{1}{2},k+\frac{1}{2}} - P_{j-\frac{1}{2},k+\frac{1}{2}})}{(\rho \Delta n)_{j-\frac{1}{2},k+\frac{1}{2}} + (\rho \Delta n)_{j-\frac{1}{2},k+\frac{1}{2}}} \qquad (16)$$

The pressure of the weak wave approximated Riemann solver(WWAM)is interpreted as

$$P_{j-\frac{1}{2},k} = \frac{(\rho c)_{j-\frac{1}{2},k-\frac{1}{2}} P_{j-\frac{1}{2},k+\frac{1}{2}} + (\rho c)_{j-\frac{1}{2},k+\frac{1}{2}} P_{j-\frac{1}{2},k-\frac{1}{2}}}{(\rho c)_{j-\frac{1}{2},k+\frac{1}{2}} + (\rho c)_{j-\frac{1}{2},k-\frac{1}{2}}} + q_{j-\frac{1}{2},k} \qquad (17)$$

WWAM Riemann solver is first proposed by Godunov [], in which the central idea is to use the simple characteristic relation to replace the shock and rarefaction relations, then the velocity and pressure can be interpreted as

$$V^{WWAM} = \frac{(\rho c)_L V_L + (\rho c)_R V_R + P_L - P_R}{(\rho c)_L + (\rho c)_R} \qquad (18)$$

$$P^{WWAM} = \frac{(\rho c)_L P_R + (\rho c)_R P_L + (V_L - V_R)(\rho c)_L (\rho c)_R}{(\rho c)_L + (\rho c)_R} \qquad (19)$$

where $U_L = (\rho_L, V_L, P_L, c_L)$ and $U_R = (\rho_R, V_R, P_R, c_R)$ are the left and right states of the Riemann solver respectively. This is the linear approximated scheme of the discontinuity decomposition, which is also called the weak wave approximated Riemann solver(WWAM).But due to much viscosity, WWAM can only simulate theproblems in which the shocks are not complex. Different approximated Riemann solver behaves different numerical features which can affect the numerical scheme for simulating the fluid flows. So we hope to analyze some practical approximated Riemann solvers for the new Lagrangian method and to simulate the complex problems. We have used several approximated Riemann solvers, for example HLLC Riemann solver, Duckowicz double shock Riemann solver and MFCAV Riemann solver, under the condition that the weight α_k is still set to the acoustic impedance, to simulate the standard numerical examples such as Sod shock tube problem, but the results are not approximated to the accuracte solution. It is shown that the Riemann solvers discussed above are not applied to the new Lagrangian method directly. Based on the consideration above, we study deeply how to develop and apply the Riemann solvers discussed above to the new Lagrangian method. For Duckowicz double shock Riemann solver which is second order accuracy and very complex, we don't consider it in this paper. But now we have found the techniques to develop and apply the HLLC and MFCAV Riemann solvers to the new Lagrangian method successfully and obtain good results. But the technique for HLLC Riemann solver is simpler compared to the one for the MFCAV Riemann solver, we don't consider it in this paper, we refer the readers to see [15] for details. In this section we will discuss deeply the technique to develop and apply the MFCAV Riemann solver to the new Lagrangian method.

A The MFCAV Approximated Riemann Solver

The MFCAV Riemann solver is practically used in many Lagrangian or ALE methods due to its merit of sharp shock profiles and rarefaction corners, though very often with numerical oscillations, see [14]. In two dimension, for such meshs displayed in Fig.4, the pressure and velocity on the normal direction of the lines in k direction, are computed by the MFCAV, which take as

$$\vec{V} \cdot n_{j-\frac{1}{2},k} = \frac{(\rho c \vec{V} \cdot n)_{j-\frac{1}{2},k+\frac{1}{2}} + (\rho c \vec{V} \cdot n)_{j-\frac{1}{2},k-\frac{1}{2}}}{(\rho c)_{j-\frac{1}{2},k+\frac{1}{2}} + (\rho c)_{j-\frac{1}{2},k-\frac{1}{2}}} - \frac{\Delta t (P_{j-\frac{1}{2},k+\frac{1}{2}} - P_{j-\frac{1}{2},k+\frac{1}{2}})}{(\rho \Delta n)_{j-\frac{1}{2},k+\frac{1}{2}} + (\rho \Delta n)_{j-\frac{1}{2},k-\frac{1}{2}}} \qquad (19)$$

World Academy of Science, Engineering and Technology
International Journal of Mathematical and Computational Sciences
Vol:5, No:5, 2011

$$P_{j-\frac{1}{2},k} = \frac{(\rho c)_{j-\frac{1}{2},k-\frac{1}{2}} P_{j-\frac{1}{2},k+\frac{1}{2}} + (\rho c)_{j-\frac{1}{2},k+\frac{1}{2}} P_{j-\frac{1}{2},k-\frac{1}{2}}}{(\rho c)_{j-\frac{1}{2},k+\frac{1}{2}} + (\rho c)_{j-\frac{1}{2},k-\frac{1}{2}}} + q_{j-\frac{1}{2},k} \qquad (20)$$

where Δt is the time interval, and $q_{j-\frac{1}{2},k}$ is the Von Neumann

artifical viscosity ,i.e.

if $(V \cdot n)_{j-\frac{1}{2},k+\frac{1}{2}} + (V \cdot n)_{j-\frac{1}{2},k-\frac{1}{2}} \geq 0$, then $q_{j-\frac{1}{2},k} = 0$; if

$(V \cdot n)_{j-\frac{1}{2},k+\frac{1}{2}} + (V \cdot n)_{j-\frac{1}{2},k-\frac{1}{2}} < 0$,then

$$q_{j-\frac{1}{2},k} = 0.5b^2((\rho c)_{j-\frac{1}{2},k+\frac{1}{2}} + (\rho c)_{j-\frac{1}{2},k-\frac{1}{2}}) \left[(\vec{V} \cdot n)_{j-\frac{1}{2},k+\frac{1}{2}} - (\vec{V} \cdot n)_{j-\frac{1}{2},k-\frac{1}{2}} \right]$$

and $n_{j-\frac{1}{2},k\pm\frac{1}{2}}$ is the normal vectors of the lines which connects

the central node of j line and $j-1$ line in cells $(j-\frac{1}{2},k\pm\frac{1}{2})$,

and points to the direction that k increases. $\Delta n_{j-\frac{1}{2},k\pm\frac{1}{2}}$ is the

distance between the central nodes of the corresponding cells and the k lines.

In (20), except for an inverse interpolate term of the weight ρc , a term of Von Neumann artifical pressure is attacted to it to modify the pressure, where b is an adjustable constant. In (19), besides an inverse interpolate term of the weight ρc , a term of acceleration is attacted to it to modify the velocity. So the MFCAVcan be adapted to the cases to which the WWAM cannot be adapted, see the comparing between MFCAV and WWAM in [14].

Similarly the pressure and velocity on the normal direction of the lines in j direction computed by the MFCAV can be seen in[14].
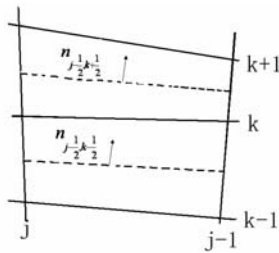

Fig. 4 the meshes

Now in the next section , we will deeply discuss the technique to develop and apply the MFCAV to the new Lagrangian method.

B The development and application of the MFCAV

1. The MFCAV in one dimension

We first discuss the technique in one dimension. From section A, in one dimension, the velocity and pressure of MFCAV can be interpreted as

$$V^{MFCAV} = \frac{\beta_L V_L + \beta_R V_R}{\beta_L + \beta_R} + \kappa_{L,R} \frac{P_L - P_R}{\beta_L + \beta_R} \qquad (21)$$

$$P^{MFCAV} = \frac{\beta_L P_R + \beta_R P_L}{\beta_L + \beta_R} + q \qquad (22)$$

where $U_L = (\rho_L, V_L, P_L, c_L)$ and $U_R = (\rho_R, V_R, P_R, c_R)$ are the left and right states of the Riemann solver respectively and

$$\beta_L = \rho_L c_L \;, \quad \beta_R = \rho_R c_R \;, \quad \kappa_{L,R} = \frac{\Delta t(\beta_L + \beta_R)}{\rho_L \Delta n_L + \rho_R \Delta n_R}$$

c_L, c_R is the sound speeds of the left and right states, Δt is the time interval, Von Neumann artifical viscousity q is

$$q = \begin{cases} 0, if\,(V_R - V_L) \geq 0 \\ 0.5b^2(\rho_R + \rho_L)(V_R - V_L)^2, if\,(V_R - V_L) < 0 \end{cases} \qquad (23)$$

Now we will discuss the technique to develop and apply MFCAV to the new Lagrangian method by viewing it as a modification of WWAM Riemann solver. We first consider the case of $q = 0$. Let

$$P * - P_L = -\beta_L (V * - V_L) + Q_L \qquad (24)$$

and

$$P * - P_R = \beta_R (V * - V_R) + Q_R \qquad (25)$$

Where Q_L and Q_R are the modification to be determined. If Q_L and Q_R are all set to be zero, then (24)and (25) are the Riemann invariants of WWAM, and the velocity and pressure of the intermidate state are (18)and (19) respectively.

From (24)and (25), the velocity and pressure of the intermidate state for MFCAV can be computed as

$$V* = \frac{\beta_L V_L + \beta_R V_R}{\beta_L + \beta_R} + \frac{P_L - P_R}{\beta_L + \beta_R} + \frac{Q_L - Q_R}{\beta_L + \beta_R} \qquad (26)$$

$$P* = \frac{\beta_L P_R + \beta_R P_L}{\beta_L + \beta_R} + \frac{\beta_L \beta_R (V_L - V_R)}{\beta_L + \beta_R} + \frac{\beta_R Q_L + \beta_L Q_R}{\beta_L + \beta_R} \qquad (27)$$

From (26)and (27) which are combined with (21)and (22),we can obtain the linear equations of Q_L and Q_R

$$Q_L - Q_R = (\kappa_{L,R} - 1)(P_L - P_R) \qquad (28a)$$

$$\beta_R Q_L + \beta_L Q_R = -\beta_L \beta_R (V_L - V_R) \qquad (28b)$$

From which Q_L and Q_R are solved out as

$$Q_L = -\frac{\beta_L \beta_R (V_L - V_R)}{\beta_L + \beta_R} + (\kappa_{L,R} - 1)\frac{\beta_L (P_L - P_R)}{\beta_L + \beta_R} \qquad (29a)$$

$$Q_R = -\frac{\beta_L \beta_R (V_L - V_R)}{\beta_L + \beta_R} + (\kappa_{L,R} - 1)\frac{\beta_R (P_R - P_L)}{\beta_L + \beta_R} \qquad (29b)$$

Similarly for the case of $q \neq 0$, Q_L and Q_R take as

$$Q_L = A - \frac{\beta_L \beta_R (V_L - V_R)}{\beta_L + \beta_R} + (\kappa_{L,R} - 1)\frac{\beta_L (P_L - P_R)}{\beta_L + \beta_R} \qquad (30a)$$

$$Q_R = A - \frac{\beta_L \beta_R (V_L - V_R)}{\beta_L + \beta_R} + (\kappa_{L,R} - 1)\frac{\beta_R (P_R - P_L)}{\beta_L + \beta_R} \qquad (30b)$$

where $A = 0.5b^2(\rho_R + \rho_L)(V_R - V_L)^2$

2. The MFCAV is applied to the new method

In this section we will applied the part 1 to the new Lagrangian method.

World Academy of Science, Engineering and Technology
International Journal of Mathematical and Computational Sciences
Vol:5, No:5, 2011

We first consider the case of $q = 0$. From the above discussion, (10) can be replaced by

$$P_{q,k}^{*,k} = P_k + \beta_k(V_q^* - V_k)N_k^{k-1} + Q_k^k \qquad (31a)$$

$$P_{q,k}^{*,k-1} = P_{k-1} - \beta_{k-1}(V_q^* - V_k)N_k^{k-1} + Q_k^{k-1} \qquad (31b)$$

Where

$$Q_k^k = \frac{\beta_k\beta_{k-1}(V_k - V_{k-1})}{\beta_k + \beta_{k-1}}N_k^{k-1} + (\kappa_{k-1,k} - 1)\frac{\beta_k(P_k - P_{k-1})}{\beta_k + \beta_{k-1}} \qquad (32a)$$

$$Q_k^{k-1} = \frac{\beta_k\beta_{k-1}(V_k - V_{k-1})}{\beta_k + \beta_{k-1}}N_k^{k-1} + (\kappa_{k-1,k} - 1)\frac{\beta_{k-1}(P_{k-1} - P_k)}{\beta_k + \beta_{k-1}}$$

(32b)

Now we substituted (31) to (11), and arrive at

$$\sum_{k=1}^{K(q)}\frac{L_k(\beta_{k-1} + \beta_k)}{}\left[V_q^* \cdot N_k^{k-1} - \frac{P_{k-1} - P_k + \beta_{k-1}V_{k-1} \cdot N_k^{k-1} + \beta_kV_k \cdot N_k^{k-1}}{\beta_{k-1} + \beta_k} - \frac{Q_k^{k-1} - Q_k^k}{\beta_{k-1} + \beta_k}\right]N_k^{k-1} = 0 \qquad (33)$$

We set, as in [1],

$$V_k^* = \frac{P_{k-1} - P_k + \beta_{k-1}V_{k-1} \cdot N_k^{k-1} + \beta_kV_k \cdot N_k^{k-1}}{\beta_{k-1} + \beta_k} + \frac{Q_k^{k-1} - Q_k^k}{\beta_{k-1} + \beta_k} \qquad (34)$$

However, in the present case, we have by noting(32)

$$Q_k^{k-1} - Q_k^k = (\kappa_{k-1,k} - 1)(P_{k-1} - P_k) \qquad (35)$$

and therefore,we have from (34)

$$V_k^* = \frac{\beta_{k-1}V_{k-1} \cdot N_k^{k-1} + \beta_kV_k \cdot N_k^{k-1}}{\beta_{k-1} + \beta_k} + \frac{\kappa_{k-1,k}(P_{k-1} - P_k)}{\beta_{k-1} + \beta_k} \qquad (36)$$

which is just the normal velocity given by the one-dimensional MFCAV Riemann solver for face $[M_q, M_k]$. With this notation, we can rewrite (33) and give an interesting interpretation of it:

$$\sum_{k=1}^{K(q)}L_k(\beta_{k-1} + \beta_k)\left[V_q^* \cdot N_k^{k-1} - V_k^*\right]N_k^{k-1} = 0 \qquad (37)$$

A straightforward calculation shows that the left-hand side of (37) is the gradient of the following quadratic functional

$$F(u_q^*, v_q^*) = \sum_{k=1}^{K(q)}L_k(\alpha_{k-1} + \alpha_k)\left[V_q^* \cdot N_k^{k-1} - V_k^*\right]^2$$

where (u_q^*, v_q^*) denotes the components of V_q^*. Consequently, the solution of (37) reaches the minimum of the functional $F(u_q^*, v_q^*)$.

From the above discussion, we note that for MFCAV compared with WWAM, the diffenece between them is that the computation of the pressure. For WWAM, the pressure is computed by (9), but the pressure of MFCAV is computed by (10).

IV. NUMERICAL EXAMPLES

In this section, we present some numerical examples of multi-material flows to demonstrate the performance of our numerical scheme. The goal of this paper is only develop and apply the MFCAV Riemann solver to the new Lagrangian method. So from the numerical examples displayed in this section we see that the numerical results not only maitain the merits such as sharp shock profiles and rarefaction corners but

also maitain the shortage such as numerical oscillations. But this shortage is not caused by the development and application, it is actually caused by the artifical viscosity which is within the range of the MFCAV applied in onther Lagrangian methods.

A One-Dimensional Examples

1 Sod's Shock Tube Problem

We consider Sod's shock tube problem in the unit interval. The initial condition is

$$(\rho, u, p, \gamma) = \begin{cases} (1, 0, 1, \frac{7}{5}), & 0.0 \le x \le 0.5 \\ (0.125, 0, 0.1, \frac{5}{3}) & 0.5 < x \le 1.0 \end{cases}$$

The computed results by WWAM and MFCAV at $t = 0.2$ are shown in Fig.5 with 400 and 20 mesh cells in x and y direction respectively, where (a), (b), (c)are the density, pressure and velocity. It is obvious that MFCAV Riemann solver exhibits a slightly better accuracy than WWAM solver near the rarefaction wave, but due to the artifical viscosity, MFCAV gives a slightly spurious osciallion near the contact discontinuity and shock wave.
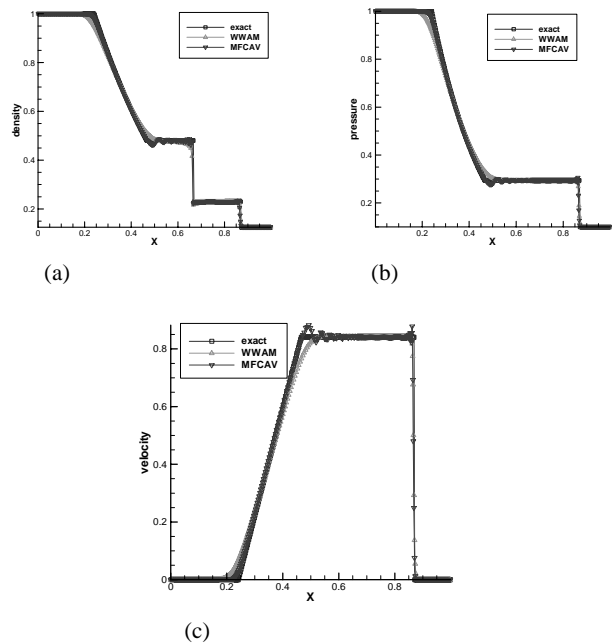

(a)

(b)

(c)

Fig.5 the results of $t = 0.2$: (a)density;(b)pressure ;(c) velocity

2 Lax' Shock Tube

The initial condition is

$$(\rho, u, p, \gamma) = \begin{cases} (0.445, 3.258, 0.698, \frac{7}{5}) & 0.0 \le x \le 1.0 \\ (0, 5, 0, 0.571, \frac{7}{5}) & 0.5 \le x \le 2.0 \end{cases}$$

The computed results by WWAMand MFCAV for Lax's problem are shown in Fig.6 with 400 and 20 mesh cells in x and y direction respectively, where (a), (b)and(c) are the

World Academy of Science, Engineering and Technology
International Journal of Mathematical and Computational Sciences
Vol:5, No:5, 2011

density, pressure and velocity. It is obvious that MFCAV Riemann solver exhibits a slightly better accuracy than WWAM solver near the rarefaction wave,contact discontinuity and shock wave, but due to the artifical viscosity, MFCAV gives a slightly spurious osciallion near the contact discontinuity and shock wave.
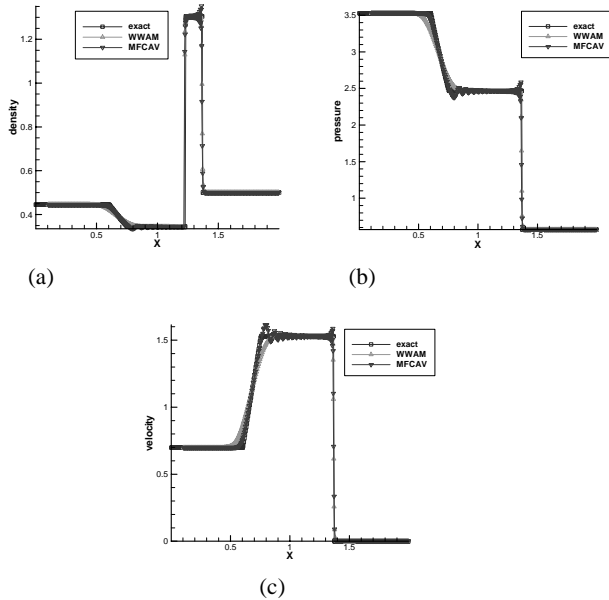

(a)   (b)

(c)

Fig.6 the results of $t = 0.15$: (a)density;(b)pressure;(c) velocity

3 Blast Wave Problem of Woodward and Colella [12]

This problem is the left part of the Woodward –Colella interacing shock wave problem, the initial condition is

$$(\rho, u, p, \gamma) = \begin{cases} (1,0,1,1000,1.4) & 0.0 \le x < 0.1 \\ (1,0,0.01,1.4) & 0.1 \le x < 0.9 \\ 1,0,100,1.4 & 0.9 \le x \le 1.0 \end{cases}$$

This problem exhibits very high pressure ratio, it is a very challenging problem for numerical methods as the compressions are exceptionally high in very small volumes. The results of $t = 0.038$ are shown in Fig.7, where (a), (b), (c) are the density, pressure and velocity respectively. It is obvious that MFCAV Riemann solver exhibits a slightly better accuracy than WWAM solver, but due to the artifical viscosity, MFCAV gives a slightly spurious osciallion.
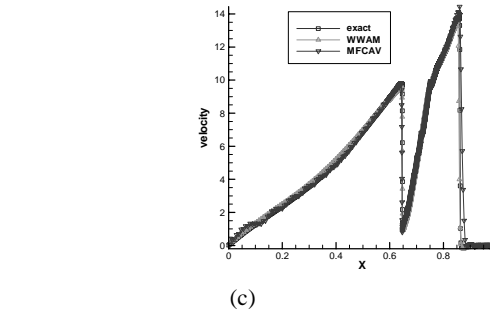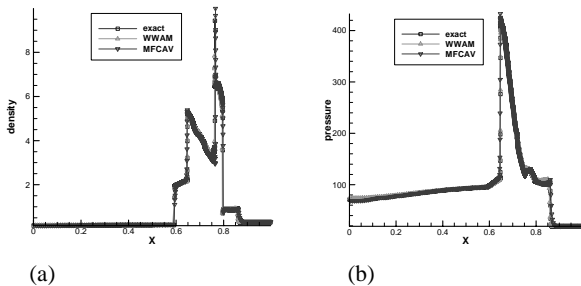

(a)   (b)

(c)

Fig.7 The results of $t = 0.038$: (a)density;(b)pressure;(c) velocity

4 Double Shock Wave Problem [10]

The initial data is

$$(\rho, u, p, \gamma) = \begin{cases} (5.99924, 19.5975, 460.894, 1.4), & 0.0 \le x \le 0.5 \\ (5.99242, -6.19633, 46.0950, 1.4) & 0.5 \le x \le 1.0 \end{cases}$$

This example with a very large pressure ratio is designed to test the robustness of numerical methods. The solution contains a left shock, a contact discontinuity, and a right shock. The results is shown in Fig.8, where (a), (b), (c) are the density, velocity and pressure. The cells in x and y direction are (400×20). We see that the numerical results are generally in good agreement with the exact solution. It is obvious that MFCAV Riemann solver exhibits a slightly better accuracy than WWAM solver, but also gives a slightly spurious osciallion.
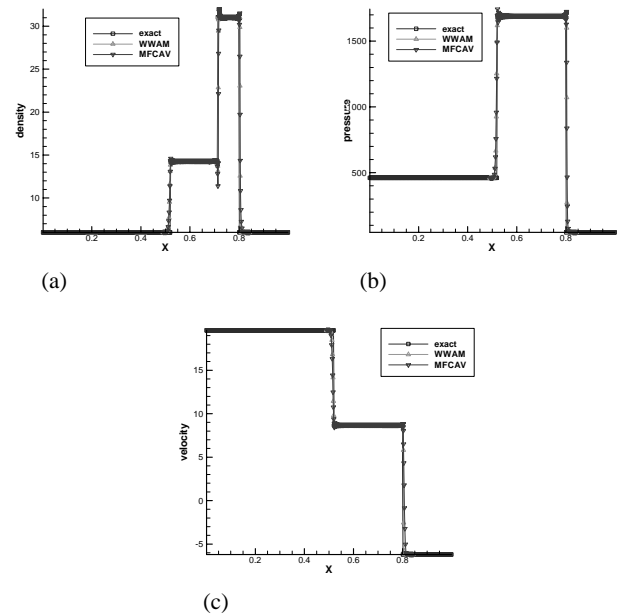

(a)   (b)

(c)

Fig.8 The results of $t = 0.025$: (a)density;(b)pressure;(c) velocity

5 Double Rarefaction Wave Problem [10]

The initial data is

$$(\rho, u, p, \gamma) = \begin{cases} (1.0, -2, 0.4), & 0.0 \le x \le 0.5 \\ (1.0, 2, 0.4), & 0.5 \le x \le 1.0 \end{cases}$$

This test also called 123 problem, has solution consisting of two strong rarefactions and a trivial stationary contact

World Academy of Science, Engineering and Technology
International Journal of Mathematical and Computational Sciences
Vol:5, No:5, 2011

discontinuity. The pressure is very small (close to vacuum), and a number of methods are known to have difficulties with this kind of symmetric Riemann problems[]. Fig.9 shows results obtained with the MFCAV and WWAM. It is obvious that MFCAV Riemann solver exhibits better accuracy than WWAM solver, specially for denstiy at rarefaction and pressure at contact.
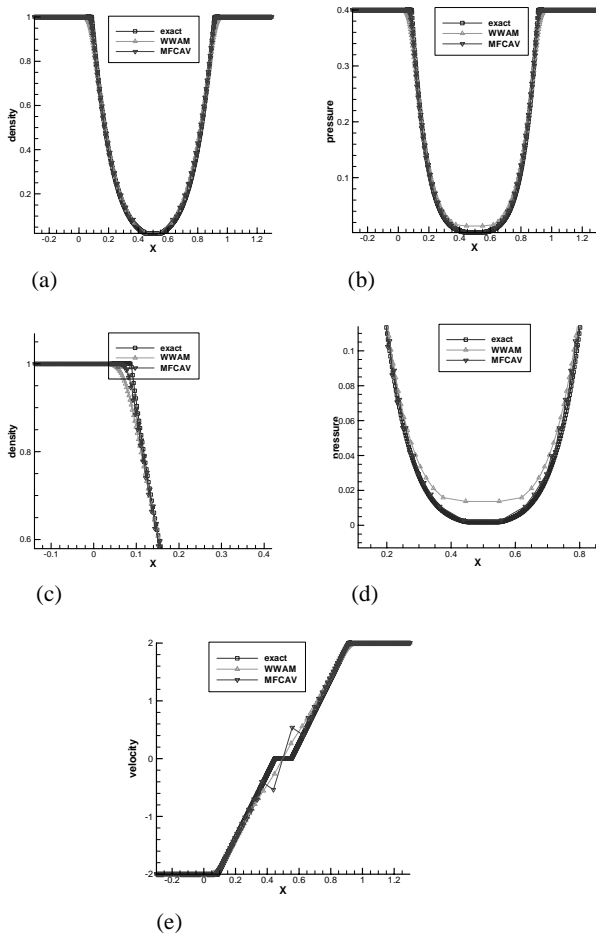

(a)

(b)

(c)

(d)

(e)

Fig.9 The solution at $t = 0.15$;(a)density ; (b)pressure; (c)The amplified figure of density at rarefaction; (d)The amplified figure of pressure at contact; (e)velocity

B Two-Dimensional Examples
1 Sedov's Blast Wave Problem

Consider a uniform medium in space with zero initial pressure. At time $t = 0$, a fixed amount of energy is deposited at the origin, $r = 0$. As time increases, a blast wave expands away from the origin. Because the initial pressure is zero, the shock associated with the blast wave is infinite in strength, and a similarity solution for the post shock profile can be obtained. The solution was first found by Sedov in 1959 for a $\gamma -$ law gas and is particularly useful for testing the accuracy of multidimensional numerical schemes [8]. Here, we run a two-dimensional calculation and compare the numerical results obtained using the Riemann solvers discussed above.

An illustrative choice for a computational mesh is the one in which the plane coordinates are $\Delta x = \Delta y = 1.1/N$ with $N = 22$ in a quadrant. A single unit of energy is deposited in the central cell of the mesh. According to the analytic theory, the blast shock wave should expand with radius equal to 1 at time $t = 1$. The results of MFCAV and WWAM Riemann solvers at time $t = 1$ is shown in Fig.10, in which   the corresponding density distributions and mesh cells are shown. The blast wave should be spherical at all times. We see that all the schemes can correctly reproduce the shape and position of the shock wave. The shock position computed by WWAM is equal to 1 at time $t = 1$. But the shock speed of MFCAVis slightly larger than the one of WWAM.
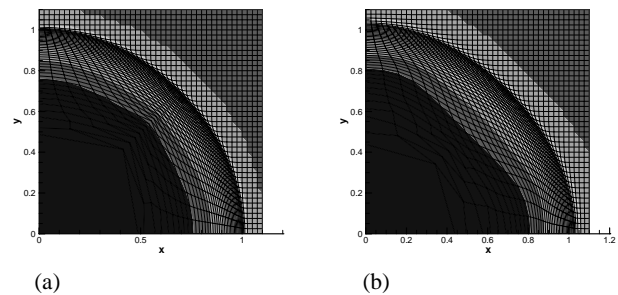

(a)

(b)

Fig.10 The results at $t = 1.0$; (a)the solution of WWAM;
(b)the solution of MFCAV

2 Noh's Test Case

Noh's test case is the implosion of a cylinder of unit radius. The cylinder is filled with a monoatomic perfect gas $(\gamma = 5/3)$. The in initial state is $(\rho^0, P^0, V^0) = (1, 0, -eR)$, where eR represents the radial unit vector. This case, defined by Noh in [11], admits a self-similar solution: a shock wave moves inwards at the constant speed $D = 1/3$.

In order to assess the robustness of our scheme, we run the Noh problem on a   Cartesian grid. This configuration leads to a more sever test case since the mesh is not aligned with the flow. We have displayed the grid and the density map in Fig.11. We note that the cylindrical symmetry is quite well preserved and that the shock is located at a circle whose radius is approximately 0.2. The grid for this test case are slightly better than those obtained by the high-order cell-centered Lagrangian scheme proposed by Mair. H.[14]. From the zoomed figure, we see that due to the spurious osciallion the flexibility of the grid computed by the WWAM is better than those obtained by MFCAV.
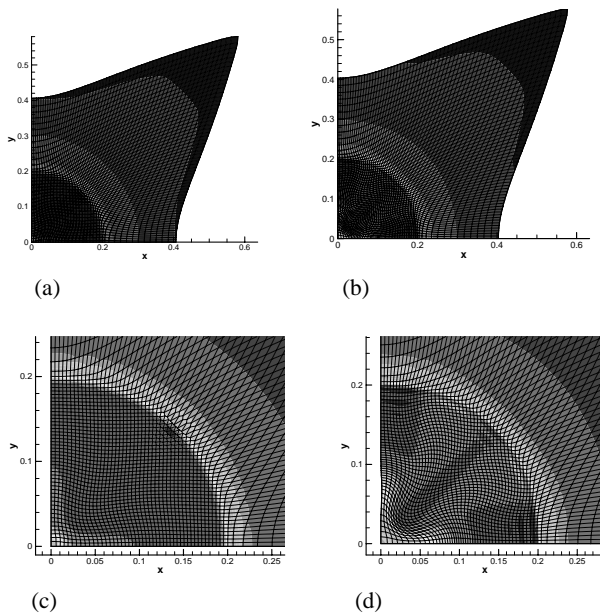
World Academy of Science, Engineering and Technology
International Journal of Mathematical and Computational Sciences
Vol:5, No:5, 2011

(a)　　　　　　　　　　(b)

(c)　　　　　　　　　　(d)

Fig.11 The mesh and density contour at $t = 0.6$; (a)the solution of
WWAM; (b)the solution of MFCAV; (c)the amplified figure of
WWAM; (c)the amplified figure of MFCAV;

Fig. 12 The mesh of initional time $t = 0.0$

(a)　　　　　　　　　　(b)
Fig. 13 The mesh at $t = 0.7$; (a)WWAM; (b) MFCAV
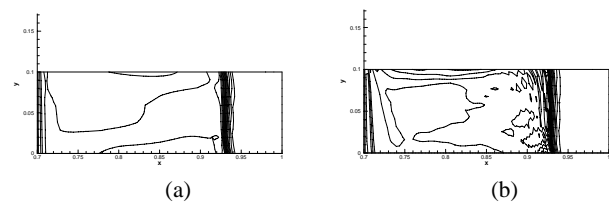
(a)　　　　　　　　　　(b)
Fig. 14 The density contour at $t = 0.7$; (a)WWAM; (b) MFCAV

3 Saltzman's Shock Tube

We consider now the movement of a planar shock wave on a
Cartesian grid that has been stretched[8]. This is a well known
difficult test case that enables to validate the robustness of our
scheme when the mesh is not aligned with the fluid flow. The
computational domain is defined by $(x, y) \in [0,1] \times [0,0.1]$.
The skewed initial mesh, shown on Fig.12, is obtained by
transforming a uniform 100×10 Cartesian grid with the
mapping

$$x_{i,j} = (i-1)dx + (11-j)dy \sin[dx(i-1)\pi]$$

$$y_{i,j} = (j-1)dy$$

$$i = 1, \cdots, 101, \; j = 1, \cdots, 11$$

$$dx = dy = 0.01$$

For the material we use the equation of state of a
monoatomic gas $(\gamma = 5/3)$. The initial state
is $(\rho^0, P^0, V^0) = (1,0,0)$. The boundary condition at $x = 0$ is a
normal velocity $v* = -1$ (inflow velocity). On all the other
boundary, we set up wall conditions.

The exact solution is a planar shock wave that moves at
speed $D = 4/3$ from left to right. Thus the shock wave hits the
face $x = 1$ at time $t = 0.75$. Behind the shock, the density is
equal to 4. We have displayed in Fig.13 and Fig.14 the density
map and the mesh at time $t = 0.7$ obtained by MFCAV and
WWAM. We note the one-dimensional solution is very well
preserved. Moreover, the location of the shock wave and the
shock plateau are in good agreement with the analytical
solution. But for MFCAV, the density contour gives some
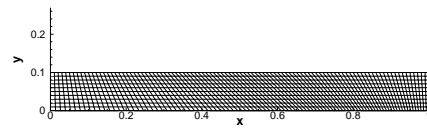spurious oscillation which caused by the artifical viscosity.

V. CONCLUSION

In a new cell-centered Lagrangian method proposed by
Maire P. H. et al [1] which possess some good new fearures
compared with calssical cell-centered Lagrangian method, we
use several Riemann solvers to simulate the standard numerical
examples such as Sod shock tube problem, but the results are
not approximated to the accuracte solution. It is shown that the
Riemann solvers are not applied to the new Lagrangian method
directly. Based on the consideration above, we study deeply
how to develop and apply the Riemann solvers to the new
Lagrangian method. By viewing it as a modification of the
WWAM Riemann solver, we apply the MFCAV Riemann
solver to the Lagrangian method. The numerical experiments
show that the application is successful in that the shock profiles
and rarefaction corners are sharpened compared with results
obtained using other Riemann solvers. Though there are still
numerical oscillations, they are within the range of the MFCAV
applied in other Lagrangian methods. The numerical
oscillations are caused by the artifical viscosity, so we will
modify the MFCAV Riemann solver by considering the
entropy to eliminate the oscillations in the future.

REFERENCES

[1] Maire P. H., Abgralll R., Breil J., et al. A cell-centered lagrangian scheme
for multidimensional compressible flow problems[J]. SIAM J. Sci.
Comput, 2007,29(4): 1781-1824
[2] Von Neumann J. and Ritchimyer R. D.. A method for the numerical
calculations of hydrodynamical shocks[J]. J. Appl. Phys.,
1950,21:232-238.
[3] Wilkins M. L., Calculation of elastic plastic flow. Methods in
computational physics[J],3,1964

World Academy of Science, Engineering and Technology
International Journal of Mathematical and Computational Sciences
Vol:5, No:5, 2011

[4] Caramana E. J., Shashkov M. J., and Whalen P. P., Formulations of artificial viscosity for multidimensional shock wave computations[J]. J. Comput. Phys.,1998, 144:70-97.

[5] Godunov S. K., Zabrodine A., Ivanov M., Kraiko A., and Prokopov G., Mir.[J], 1979.

[6] Richtmyer R. D. and Morton K. W., Differencd methods for initial-value problems. John Wiley, 1967

[7] Duckowicz J. K., Bertrand J. A. Meltz. Vorticity errors in multidimensional Lagrangian codes [J].Comput. Phys,1992, 99:115-134.

[8] Addessio F. L., et,al. CAVEAT: A computer code for fluid dynamics problem with large distortion and internal slip[M], Los Alamos report LA-10613-MS,1992.

[9] Tian B, Shen W, Liu Y, etal, Numerical study on several Godunov-type schemes with AlE formulation. Computational physics(Chinese Journal): 2007,24(5):537-542.

[10] Toro E. F., Riemann solvers and numerical methods for fluid dynamics, A Practical Introduction, 2nd edition,Spring-verlag,1999.

[11] W. F. Noh, Errors for calculations of strong shocks using artifical viscosity and artifical heat flux. J.Comput. Phys., 72:78-120,1987.

[12] P. Woodward and P. Colella, The numerical simulation of two-dimensional fluid flow with strong shocks. J.Comput. Phys., 54:115-173,1984.

[13] MAIRE P H, A high order cell-centered Lagrangian scheme for two-dimensional compressible fluid flows on unstructured meshes.

[14] Li D, Xu G, Shui H, et.al., Numerical Methods for Two-dimensional Unsteady Fluid Dynamics. The Science Press: Beijing, 1987; 246..

[15] Yan Liu, Baolin Tian, Weidong Shen, Comparing study on two approximated Riemann solvers in a new cell-centered Lagrangian method, GF report (GF-A0128959G),2010 (in Chinese).

Yan Liu was born in 1974 and has earned doctoral degree of numerical methods of conservation laws from Shanghai University, Shanghai, China, in 2004. Now she major in numerical methods of compressible dynamics fluids.